Materials Today Sustainability 31 (2025) 101158

Contents lists available at ScienceDirect

Materials Today Sustainability

journal homepage: www.journals.elsevier.com/materials-today-sustainability

Water-driven photovoltaics: Enhancing performance through water media in the active layer

Malkeshkumar Patel [a,b], Md Arifur Rahman Barno [a,b], Jessica Barichello [c], Sanh Vo Thi [a,b], Seunghee Cho [a,b], Fabio Matteocci [d], Aldo Di Carlo [c,d,*], Ching-Ping Wong [e,**], Joondong Kim [a,b,***]

[a] Photoelectric and Energy Device Application Lab (PEDAL), Multidisciplinary Core Institute for Future Energies (MCIFE), 119 Academy Rd. Yeonsu, Incheon, 22012, Republic of Korea
[b] Department of Electrical Engineering, Incheon National University, 119 Academy Rd., Yeonsu, Incheon, 22012, Republic of Korea
[c] ISM-CNR, Istituto di Struttura della Materia, Consiglio Nazionale delle Ricerche, Via del Fosso del Cavaliere 100, 00133, Roma, Italy
[d] CHOSE, Centre for Hybrid Organic Solar Energy, Department of Electronic Engineering, University of Rome, Tor Vergata, Via del Politecnico 1, 000133, Roma, Italy
[e] School of Materials Science and Engineering, Georgia Institute of Technology, Atlanta, GA, 30332, United States

ARTICLE INFO

Keywords:
Solar cells
Water immersion
Thermal management
Light management
Stable onsite power

ABSTRACT

Complex design strategies aimed at mitigating optical and thermal losses have resulted in significant improvements in the photovoltaic (PV) technology. However, these strategies often entail increased processing time, device complexity, and system cost. To address these limitations, a simple water-immersion strategy for silicon solar cells is proposed in this study. The water layer, with a low refractive index and in direct contact with the solar cell, reduces Fresnel reflectance and enhances light trapping, leading to improved diode and photovoltaic characteristics. Under standard AM1.5 illumination, the commercial PV cells in air, steady water, and flowing water show power conversion efficiencies (PCEs) of 20.41 %, 23.42 %, and 22.87 %, respectively. With the optimal water depth, the cell in flowing water shows significantly enhanced and consistent onsite power generation, with the variation below 1 %. The immersion method also improves device performance across various light illumination wavelengths and intensities, maintaining a high PCE at 850 nm. The temperature of the solar cell in flowing water remained at 17 °C, ensuring high and reliable onsite power. This simple and cost-effective method presents as a promising high-performance and reliable strategy for solar power generation and may contribute significantly to the widespread deployment of renewable energy.

1. Introduction

Si solar cells have dominated the photovoltaic (PV) industry for decades owing to their abundance, mature technology, and relatively high efficiency [1–4]. Despite these advantages, their performance is still constrained by their limited optical absorption and associated thermal losses. Significant efforts have been made to address these challenges. Thus, various design innovations, material combinations, and complex processing techniques have been proposed [5–13].

One of the primary strategies for improving the efficiency of Si solar cells is the development of anti-reflection (AR) coatings, which effectively enhance light utilization, resulting in enhanced power generation and energy conversion efficiency, even under a fixed light intensity and the limited incident angle on the Si light absorber. However, the reflective losses at the air-silicon interface can significantly reduce the amount of light absorbed by the solar cell, thereby limiting their power output [14,15]. To mitigate this issue, AR coatings, typically composed of silicon nitride (SiN_X) or other dielectric materials [16–18] are applied to the cell surface to minimize reflectance across a broad range of wavelengths [19]. These coatings are designed to match the refractive indices of air and the silicon system, thereby reducing Fresnel losses and enhancing light absorption. While AR coatings have proven to

* Corresponding author. ISM-CNR, Istituto di Struttura della Materia, Consiglio Nazionale delle Ricerche, Via del Fosso del Cavaliere 100, 00133, Roma, Italy.
** Corresponding author. School of Materials Science and Engineering, Georgia Institute of Technology, Atlanta, GA, 30332, United Sates.
*** Corresponding author. Photoelectric and Energy Device Application Lab (PEDAL), Multidisciplinary Core Institute for Future Energies (MCIFE), 119 Academy Rd. Yeonsu, Incheon, 22012, Republic of Korea.
E-mail addresses: aldo.dicarlo@artov.ism.cnr.it (A. Di Carlo), cp.wong@mse.gatech.edu (C.-P. Wong), joonkim@incheon.ac.kr (J. Kim).

https://doi.org/10.1016/j.mtsust.2025.101158
Received 8 May 2025; Received in revised form 5 June 2025; Accepted 14 June 2025
Available online 19 June 2025

be effective in improving light management, they add complexity to the fabrication process and often require that the thickness and uniformity of the coating layers be accurately controlled to optimize the performance of the PV cell across different operating conditions.

In addition to AR coatings, nanotechnology has emerged as a powerful strategy for improving solar cell performance [20,21]. Modifying solar cell device architecture using nanostructures, such as quantum dots [21], plasmonic nanoparticles [22], and surface texturing [23,24] have shown great promise for enhancing light trapping and minimizing recombination losses. By integrating nanostructures directly into the cell design, researchers have identified more efficient pathways for charge-carrier collection and have also successfully reduced the overall losses associated with charge recombination. For example, surface texturing techniques [25] that introduce nanoscale roughness or periodic patterns [26] can significantly increase the effective surface area of PV cells, thereby enhancing their ability to capture and absorb incoming light. These nanostructured surfaces can also scatter light, allowing the light to bounce within the cell, thereby increasing the likelihood of photon absorption.

Nanowires have been explored as an additional means for enhancing the performance of Si solar cells. Nanowires, typically composed of Si or other semiconducting materials, can be incorporated into solar cell structures to improve charge carrier separation and transport [27–29]. Further, the high aspect ratio of nanowires allows for efficient light absorption over a broad spectrum and their vertical alignment facilitates rapid charge extraction and reduces recombination losses. The integration of nanowire arrays into Si solar cells has shown the potential to significantly improve the overall power conversion efficiency (PCE) of solar cells, particularly under low-light or diffuse illumination conditions [28,29]. However, the fabrication of nanowire-based solar cells introduces further complexity because precise control over the size, shape, and density of the nanowires is required to achieve optimal performance.

Although innovations in AR coatings, device architecture, and nanostructure integration have led to predictable improvements in solar cell performance, these strategies present significant challenges related to processing complexity and material integration. Combining different materials with varying optical and electrical properties often necessitates multistep fabrication processes that can be time-consuming and costly. For example, the deposition of AR coatings followed by the incorporation of nanostructures [28–30], often involves a series of lithographic and chemical vapor deposition techniques that must be carefully controlled to ensure desired material properties and device performance. Moreover, the integration of dissimilar materials, such as metals and semiconductors can cause additional issues such as interface defects and carrier recombination sites, which can negatively impact the overall efficiency of the device.

In addition to the effect of AR on light modulation, thermal concerns are critical for ensuring photovoltaic power generation under light exposure. When light interacts with solar cells, photon energy exceeding the band gap is converted to heat via thermalization. The infrared (IR) portion of the electromagnetic spectrum contributes to heating by inducing vibration in the atomic lattice. Additionally, high-energy photons with energies above the bandgap of the light-absorbing entity can induce thermal degradation via non-radiative losses owing to relaxation energy that is not fully converted to electricity. Thermalization losses induce rapid increases in temperature, and thus, degrade solar cell performance by introducing parasitic losses that significantly reduce the open-circuit voltage (V_{OC}) and fill factor (FF), and consequently, the PCE [8,30–33]. Further, owing to thermalization, the temperature of solar devices can increase from 28 to 80 °C under sunlight, lowering output power by −0.65 % K^{-1} and PCE by −0.08 % K^{-1} for single-crystalline Si solar cells [34,35]. Standard solar cell modules consist of a backsheet and glass, which are thermal insulators that further intensify increases in temperature owing to poor heat dissipation, resulting in the module temperature reaching 88 °C [36]. Under field conditions with the solar irradiance at 100 mW cm^{-2}, the temperature of solar modules can reach 70 °C and an environmental temperature of 50 °C can induce economic impacts due to the thermal effects on the PV system during peak solar irradiance [37]. To mitigate heat-related power losses and performance degradation, various active and passive cooling methods have been proposed. These include water and air cooling, the use of phase-change materials, floating systems, water pipes, and water sprayers, geothermal cooling, and natural convection [8,38–43]. Moreover, immersion solutions have been explored—such as ethanol, dimethyl silicon oil, ethyl acetate, distilled water, and tap water—to maintain a stable thermal state of solar cell modules [44–46]. However, these strategies remain insufficient to ensure adequate power generation.

Thus, there has been growing interest in exploring more effective strategies for improving the performance of Si solar cells without the need for complex processing or material combinations [1,47]. In this context, the use of water immersion as a passive light management and thermal dissipation technique has emerged as a promising alternative [38,48–56]. Water, with its low refractive index and excellent thermal conductivity [57–59], offers a simple yet effective strategy for reducing Fresnel reflectance and managing the thermal load of solar cells during operation [60]. It is worthy of mansion that tap water, distilled water, and seawater has been examined for the Si solar cell modules for domestic [40,52,55] and underwater applications [61–63]. Furthermore, Chow et al. proposed PV water glazing to include harvest thermal loss of solar module for the building integrated applications [64–66].

However, it remains unclear whether water can be transformed from a passive cooling or unwanted entity into an active component of PV systems. Table 1 summarizes various immersion strategies for solar cells along with potential techniques for improving power conversion efficiencies, providing a benchmark for this study. By immersing Si solar cells in water, it is possible to not only enhance light trapping but also maintain lower operating temperatures. This approach can improve the overall stability and reliability of the device, in addition to enhancing power generation.

In this study, we investigated water immersion as a novel method for enhancing the performance of Si solar cells. Our experiments showed that water immersion significantly enhanced PCE under both steady and flowing water conditions (23.42 % and 22.26 %, respectively) under standard light illumination at a wavelength of 850 nm. A water-gated Si photovoltaic (PV) system was also developed to enhance power generation by modulating light management and thermal treatment. Thus, we observed that the water layer reduced Fresnel reflectance by matching refractive indices, allowing greater light absorption and conversion to electrical energy. These results highlight water immersion as a simple, scalable, and cost-effective strategy for enhancing the efficiency and reliability of Si solar cells. In a world increasingly driven to replace fossil fuels with clean and renewable energy across diverse sectors, the findings from our study unveil novel frontiers for photovoltaic applications that have received limited attention but are generating growing interest within the scientific community [67]. Submerging photovoltaic systems just a few centimeters beneath the water's surface presents a promising advancement in the field of floating PV, enhancing PCE and providing significant cooling benefits, as demonstrated by our research.

2. Results and discussion

2.1. Water immersion Si solar cell for broadband solar energy harvesting

The AM1.5G solar irradiance spectrum (Fig. 1a) provides a critical baseline for understanding the performance of solar cells under standard test conditions. The spectrum spans the ultraviolet (UV) to near-infrared (NIR) region and shows peak intensities in the visible range. This distribution is essential for evaluating the efficiency of solar cells as it captures the solar energy available for conversion into electrical energy. This spectrum also aids in the design of solar cells that maximize

Table 1
Summary of immersion strategies for silicon solar cells using various techniques to improve power conversion efficiency.

Device structure	Immersion solution	Improvements in PCE (%)	Study			Strategy	Year/Ref.
			Optical	Electrical	Thermal		
Si solar cell module with EVA encapsulation	Ethanol Silicon oil Tap water	–	✓	×	×	Passive	2009/[44]
CPV-Mono-crystalline Si solar cell module	Flowing DI water	–	×	×	✓	Passive	2011/[48]
CPV-Mono-crystalline Si solar cell module	Flowing DI water	7.4 % to 8.2 %	×	✓	✓	Passive	2012/[43]
CPV-Mono-crystalline Si solar cell module	DI water IPA Silicon oil Ethyl acetate	17.9 % to 19.4 % 18.7 % to 21.7 % 17.6 % to 19.4 % 18.2 % to 19.8 %	×	✓	✓	Passive	2013/[45]
CPV-Mono-crystalline Si solar cell module	Dimethyl silicon oil	–	×	✓	✓	Passive	2014/[46]
a-Si based thin film PV module	Tap water	–	×	✓	×	Passive	2019/[50]
Mono-Si poly-Si a-Si module	DI water Tap water Lake water Seawater	–	×	✓	×	Passive	2021/[63]
Mono-Si a-Si module	DI water Tap water Seawater	–	×	✓	×	Passive	2020/[62]
poly-Si module	DI water Tap water Seawater	–	×	✓	×	Passive	2020/[61]
poly-Si module	Tap water	14.25 % to 15.54 %	×	✓	✓	Passive	2021/[55]
Mono-Si module	Tap water	–	×	✓	✓	Passive	2022/[40]
Mono-Si module	Tap water	–	×	✓	✓	Passive	2023/[52]
poly-Si solar cell (n + p junction with SiN_X)	Steady tap water Flowing tap water	20.41 % to 23.42 %	✓	✓	✓	Active	This study

sunlight absorption across the entire range. The inset of Fig. 1a illustrates the various energy conversion processes within an ideal single-junction Si solar cell. It shows the different losses and efficiencies of the solar cell, including solar spectrum absorption (100 mW cm^{-2}), non-absorbed light (19 mW cm^{-2}), thermalization (33 mW cm^{-2}), electrical losses (15 mW cm^{-2}), and available electrical power (33 mW cm^{-2}) [21]. This breakdown highlights the importance of minimizing optical and thermal losses to enhance the overall efficiency of solar cells.

Over the years, the use of AR coatings has become common practice in solar-cell design to improve light management and overall performance [17,68,69]. As shown in Fig. 1b (left panel), a commercial p-n^+ junction Si solar cell is designed with a SiN_X AR coating to reduce the inevitable reflectance of incident light at the surface of the cell and thereby increase light absorption.

Water with a lower refractive index than SiN_X or glass introduces an optical interface that guides incident light more effectively [50,52,55,70,71]. Fig. 1b (right) shows a Si solar cell with an additional water layer to minimize reflection and guide incident light at various incident angles. This layer enhances light penetration into the device and broadens the range of guided light angles; thus, significantly improves the performance of the solar cell for real-world application, characterized by a significant variation of the sunlight incident angle throughout the day [72]. By optimizing the design for different incident angles, the solar cell can achieve a more stable performance as well as a higher overall efficiency.

To determine the total amount of reflected light at the cell surface, we used Fresnel equations [73], which describe the reflection and transmission of light at the boundary between two media. Under normal incidence, the reflectance R, was calculated using according to the following equation:

$$R = \left(\frac{n_1 - n_2}{n_1 + n_2}\right)^2 \tag{1}$$

where n_1 and n_2 denote the refractive indices of the first and second media, respectively. For non-normal incidence, the reflectance becomes more complex and depends on the angle of incidence (θ).

$$R = R_{\perp} + R_{\sim} \tag{2}$$

where $R_{\perp}$ and $R_{\sim}$ represent the reflectances of p-polarized (parallel) and s-polarized (perpendicular) light, respectively. Further, the equations for calculating $R_{\sim}$ and $R_{\perp}$ are given by:

$$R_{\perp} = \left(\tan\left(\frac{\theta - \theta_1}{\tan(\theta + \theta_1)}\right)^2 \tag{3}$$

$$R_{\sim} = \left(\sin\left(\frac{\theta - \theta_1}{\sin(\theta + \theta_1)}\right)^2 \tag{4}$$

where θ_1 represents the angle of refraction according to Snell's law:

$$n_1 \sin(\theta) = n_2 \sin(\theta_1) \tag{5}$$

Fig. 1c shows the air-to-Si, air to SiN_X and air-to-water Fresnel reflection profiles of the solar cell used in this study. From this figure, it is evident $R_{\perp}$ and $R_{\sim}$ decreased across various incident light angles due to the formation of an effective optical interface by the water layer.

Further, Fig. 1d shows the total reflected light for various incident

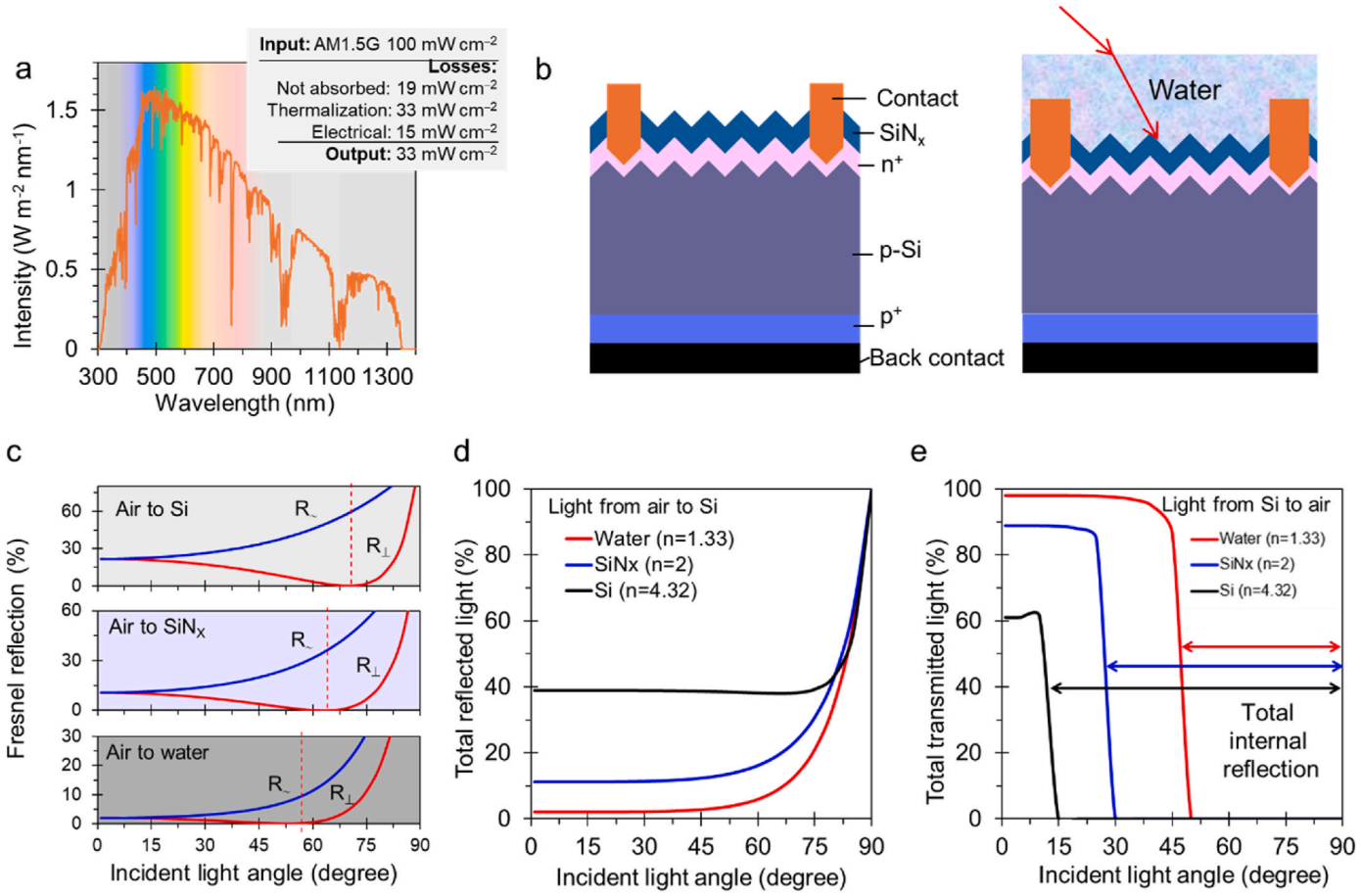

Fig. 1. Broadband solar energy harvesting using a water-immersed Si solar cell. (a) Solar irradiance of AM1.5G and breakdown of energy conversion processes for an ideal single-junction Si solar cell. (b) Schematic representation of a commercial Si solar cell with an SiN_X anti-reflection coating and a water layer for light absorbance at various incident angles. (c) Fresnel reflection profiles of light polarized in parallel ($R_\perp$) and perpendicular ($R_\parallel$) to the surface in terms of the incident light angle. Top panel, air-Si interface; middle panel, air-SiN_X interface; and bottom panel, air-water interface. The vertical line shows the incident light angle corresponding to the Brewster's angle at which Fresnel reflection on the RP becomes minimum. In calculations, we used 1, 1.33, 2, and 4.32 as the refractive indices of air, water, SiN_X, and Si, respectively. (d) Total reflected light for various incident light angles at the air-Si and water-SiN_X interfaces. (e) Total transmitted light for various incident light angles with light traveling from Si to air through the SiN_X and water layers.

light angles when light traveled from air to Si through the water and SiN_X layers. From this Figure, it is evident that the water layer significantly reduced reflectance from 40 % to <2.2 % across a wide range of incident angles (0–45°). This decrease in reflectance is crucial for enhancing the light-trapping efficiency of solar cells, as it allows more light to be absorbed and converted into electrical energy throughout the day. The use of the water layer in conjunction with the SiN_X AR coating further improved the overall light management.

As shown in Fig. 1d, the decrease in the total reflected light can be attributed to the combined effect of the SiN_X AR coating and the water layer. The SiN_X coating minimized reflectance at the air-Si interface (from 40 % to 11.1 %), whereas the water layer further reduced reflectance (from 11.1 % to 2.1 %) by matching the refractive indices more closely, thereby minimizing light reflection at the Si-water interface. Upon adding water dropwise to the Si cell, we observed a rapid change in color from blue to black. This color change further confirmed a significant decrease in light reflection at the water interface.

Fig. 1e shows the total amount of transmitted light for various incident light angles at the Si-air and SiN_X-water interfaces. The plot indicates that the water layer helped to maintain higher transmission rates, even at different angles. This improved transmission enabled the solar cell to utilize the maximum amount of light. Additionally, by enhancing light transmission through the cell, the water layer improved the overall performance of the solar cell.

2.2. Diode properties and performance of the water-immersed solar cell

In this study, we examined the performance of the water-immersed solar cell, focusing on diode characteristics (dark saturation current (J_0) and diode ideality factor (n)), and solar cell performance as compared to current conventional coating system of SiN_X for Si solar cells. We also examined the current density-voltage (J-V) characteristics of the device. Fig. 2a shows a comparison of the dark current density (J) values of a cell operated in air with that immersed in water at 25 °C, with the water layer considered to be part of the device (inset in Fig. 2a). Further, given that the dark current density values of a solar cell are determined by its normal p-n junction behavior, they can be used to determine diode characteristics

$$J = J_0\left(e^{\left(\frac{qV}{nkT}\right)} - 1\right) \tag{6}$$

where V, k, T, and q represent applied voltage, Boltzmann constant, temperature, and elementary charge, respectively.

Fig. 2b and c show the J_0 and n values of 12 devices in air and water, respectively. From these results, it is evident that water immersion lowered the J_0 values of the cells from 6.3×10^{-7} to 1.6×10^{-8} A cm^{-2} (Table S1), implying fewer recombination currents [16]. Further, the diode ideality factor for the water-immersed cells improved from 1.8 to

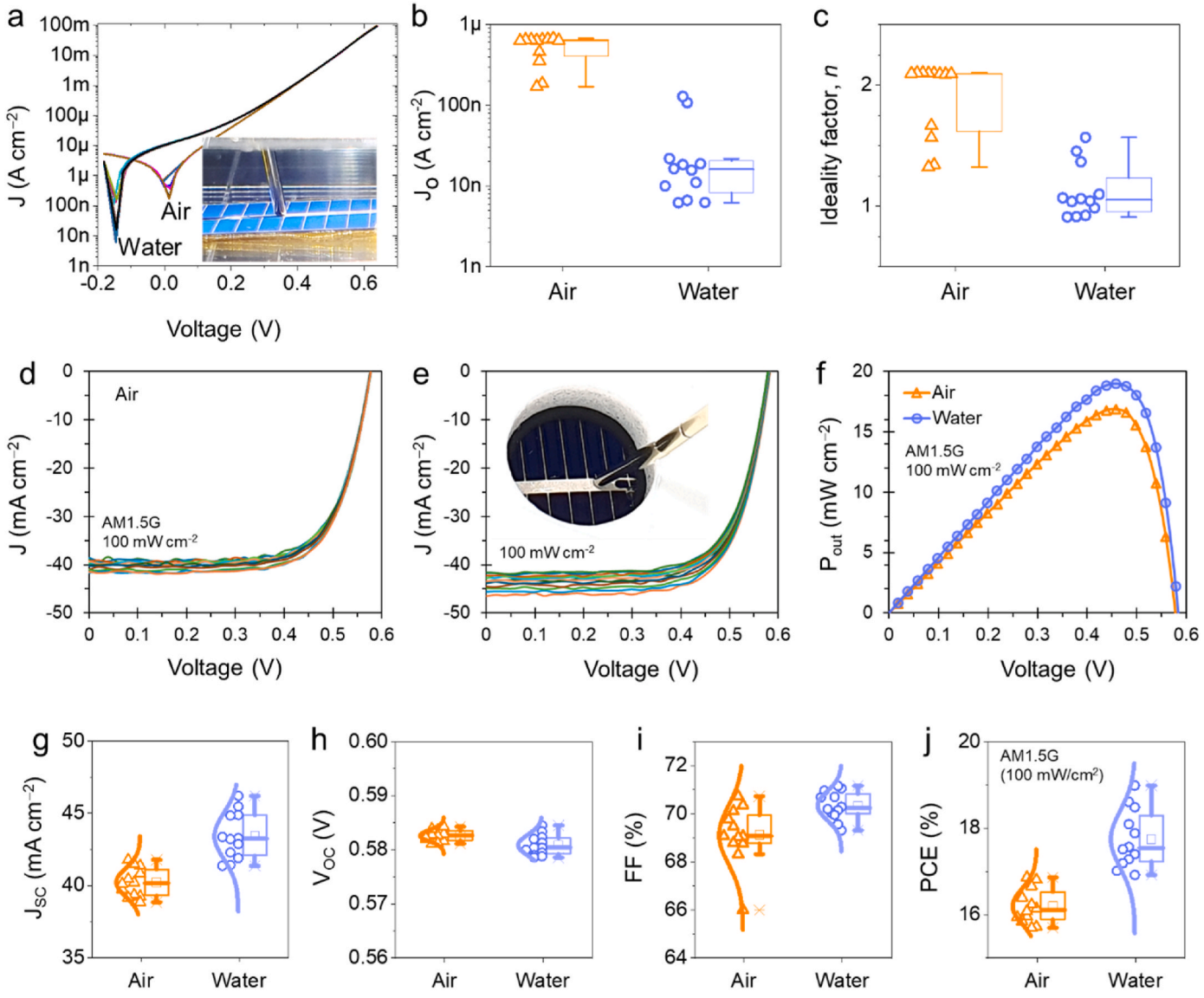

Fig. 2. Diode characteristics of Si cells in air and water. (a) Current density-voltage (J–V) characteristic of Si PV device in air and underwater for dark conditions at 25 °C. Summary of (b) Dark saturation current (J_0), and (c) Diode ideality factor (n) of the Si PV device in air and underwater. J-V characteristic of devices under standard AM1.5G illumination (100 mW cm^{-2}) in (d) Air and (e) Water. A total of 12 devices were examined using the O-ring assembly, as shown in the inset. (f) Power density-voltage (P–V) characteristic of solar cells in air and water under AM1.5G illumination. Summary of the distribution of PV cell performance parameters: (g) Short-circuit current (J_{SC}), (h) Open-circuit voltage (V_{OC}), (i) Fill factor (FF), and (j) Power conversion efficiency (PCE).

approximately 1, indicating a more ideal diode behavior. Therefore, the distribution of the J_0 and n values for the Si devices in air and water confirmed minimal recombination currents and improved diode characteristics owing to the presence of the water layer.

To confirm the solar cell performance improvement effects of the water layer, the J-V characteristics of the devices were measured under standard AM1.5G illumination (100 mW cm^{-2}). The solar cells in air (Fig. 2d) and underwater (Fig. 2e) showed downward shifts in dark current, consistent with the variation of the photocurrent, which depends on light intensity. However, the water-immersed device showed significantly enhanced current and voltage values, implying a higher PCE. This output power enhancement was also confirmed by the power density-voltage (P–V) characteristics of the water-immersed device as shown in Fig. 2f and highlights the power output (P_{out}) under standard illumination for the device in air and under water. Notably, the Pout of the device in air and water were 16.86 and 18.98 mW cm^{-2}, respectively. This improvement could be attributed to enhanced photovoltaic performance parameters, including the short-circuit current (J_{SC}), V_{OC}, and FF, as well as the better thermal management provided by the water layer.

For solar cells in practical application, J_{SC}, V_{OC}, FF, and PCE are calculated as follows:

$$J_{SC} = J_{ph} - I_o\left(e^{\frac{qV}{nkT}} - 1\right) \tag{7}$$

$$V_{OC} = \frac{kT}{q} ln\left(1 + \frac{J_{SC}}{J_0}\right) \tag{8}$$

$$FF = \frac{J_m V_m}{J_{SC}\ V_{OC}} = \frac{P_{max}}{J_{SC}\ V_{OC}} \tag{9}$$

$$PCE = \frac{J_{SC}\ V_{OC}\ FF}{P_{hv}(AM1.5G)} \tag{10}$$

where J_{ph} represents photocurrent density; J_m and V_m represent the maximum current density and voltage values, respectively, P_{max}

represents the maximum power density; and P_{hv} represents light intensity. Given that J_0 is negligible relative to J_{ph}, we considered J_{SC} as equal to J_{ph}.

Fig. 2g–j summarizes the distribution of crucial PV performance parameters, including J_{SC}, V_{OC}, FF, and PCE, respectively, showing that water immersion resulted in higher performance metrics across the device array. The PV parameters are tabulated in Table S2. As previously confirmed, water immersion reduced Fresnel reflectance and improved light trapping, thereby enhancing J_{SC} owing to an increased light flux. The reduced reflectance allowed more light to be absorbed by the silicon layer, increasing the number of generated charge carriers and, thus, J_{SC}. Further, improving J_{SC} also improved the V_{OC}, FF, and PCE.

To evaluate the performance of PV devices, it is also crucial to consider the parasitic losses that occur due to electrical losses (series resistance, R_S) and recombination losses at the junction interface (shunt resistance, R_{sh}) based in the relationship below.

$$J_{SC} = J_{ph} - I_o\left(e^{\frac{q(V-IR_S)}{nkT}} - 1\right) - \frac{V - IR_S}{R_{sh}} \tag{11}$$

According to the above equation, improvements in J_{SC} are reflective of the underlying importance of R_S and R_{sh} improvements owing to water immersion. From Fig. 2, it is evident that water immersion significantly enhanced the electrical properties and overall efficiency of the p-n junction Si PV devices. Improvements in J_{SC}, V_{OC}, FF, and PCE, alongside the decrease in the J_0 value and a more ideal diode behavior, highlight the beneficial effects of water immersion.

2.3. Effect of immersion depth and light intensity on device performance

In this study, we also investigated the effects of water layer thickness and light intensity on the performance of the Si solar cells. The water layer thickness was controlled using an O-ring assembly, which defined the active area of the device and isolated the emitter and real metal contacts.

The J-V and P–V characteristics of Si PV devices at different water depths (up to 29 mm) under standard AM1.5G illumination are shown in Fig. 3a and b. From Fig. 3a, it is evident that increasing water layer thickness resulted in improvements in J_{SC} and V_{OC} up to a certain threshold, beyond which the J_{SC} and V_{OC} values plateaued or declined slightly. This trend was also evident in the P–V curves shown in Fig. 3b, with the PCE peaking at an optimal water-layer thickness. This behavior can be attributed to the balance between reduced Fresnel reflectance and enhanced light trapping at the optimal thickness, which maximized light absorption within the silicon layer owing to internal reflection by the water layer. The reduced reflectance and multiple reflections allowed the absorption of more light by the silicon layer, resulting in an increase in the number of generated charge carriers and thus the value of Jsc. This observation can be clarified considering the relationship between photon flux (ϕ), reflectance, internal quantum efficiency (IQE), and J_{SC}, as shown below. The variation of PV parameters as a function of water layer thickness (Fig. S1) also confirmed stable V_{OC} and FF values of 0.58 V and 70 %, respectively, throughout the measurements.

$$J_{SC} = q\int_{(\lambda)} \phi(\lambda)\,(1 - R(\lambda))IQE(\lambda)d\lambda \tag{12}$$

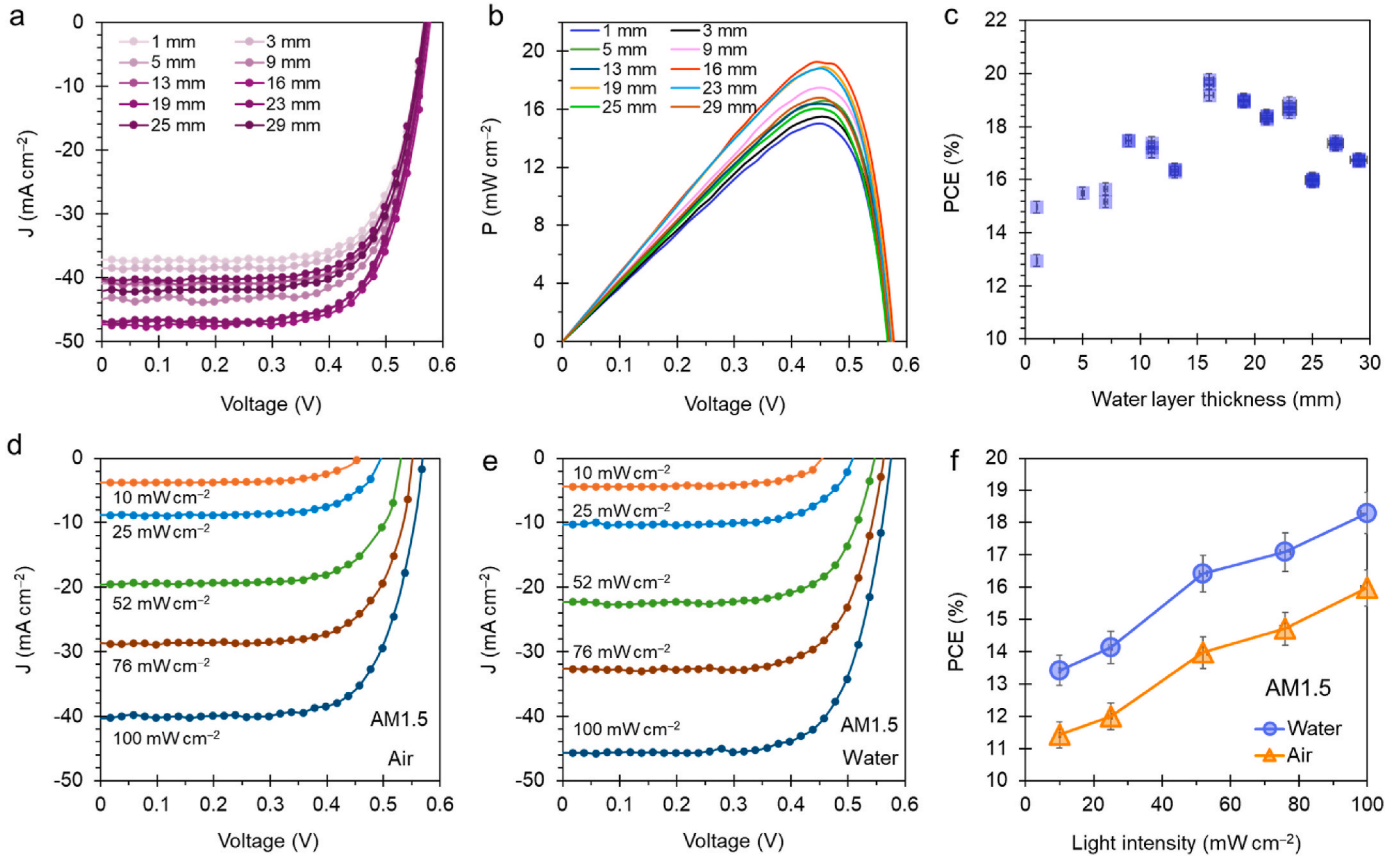

Fig. 3. Effects of water layer thickness and light intensity on the performance of PV cells. (a) Current density-voltage (J–V) characteristics, and (b) Power density-voltage (P–V) characteristic plots of Si PV devices under different water layer thicknesses, varied from 1 to 29 mm using the O-ring assembly cell (tap water was used for the experiment). (c) Power conversion efficiency (PCE) of Si PV devices under different water layer thickness conditions. J-V characteristic of Si PV device operation in (d) Air and (e) Water under AM1.5 illumination in the range 10–100 mW cm^{-2}. The device temperature was set at 25 °C. (f) Power conversion efficiency (PCE) of device under different light intensities (AM1.5 in the range 10–100 mW cm^{-2}).

Fig. 3c provides a summary of PCE as a function of water layer thickness. From this figure, it is evident that PCE increased with increasing water layer thickness up to an optimal point (approximately 15 mm) and thereafter, declined slightly. This optimal thickness is crucial for minimizing reflectance and maximizing light trapping, as discussed earlier. Additionally, beyond this optimal thickness, the additional water layer did not bring about any significant improvement in light absorption, but increased light travel distance light, leading to light loss owing to scattering.

The optimal water layer thickness was considered to confirm the effect of water immersion under varying light illumination intensities on solar cell performance. The J-V characteristics of Si PV devices in air and water under AM1.5G illumination in the range 10–100 mW cm^{-2} are shown in Fig. 3d and e. The increased J_{ph} value resulting from the shift in the J-V plot data showed that water immersion consistently enhanced J_{SC} across different light intensities. The light intensity versus J_{SC} relationship also confirmed the recombination process [74]. By applying power law fitting based on $J_{SC} \alpha P_{hv}^{\alpha}$, with α representing the recombination process and trapping of an electron–hole pair in the semiconductor material, the α value approached unity (1) suggesting fewer recombination states and less trapping of photogenerated carriers. PV devices in air and water showed α values of 1.02 and 1.001, respectively, implying fewer recombination sites and less trapping of photogenerated carriers (Fig. S2). This observation also confirmed improvements in V_{OC} and FF with increasing light intensity for the device in both air and water.

Fig. 3f illustrates PCE as a function of light intensity for devices in air and water. Notably, PCE increased with light intensity under both conditions, but the water-immersed devices exhibited a higher PCE across all intensities. This improvement can be attributed to the reduced reflectance and better light and thermal management provided by the water layer.

These results emphasize the potential of water immersion in mitigating optical and thermal losses, leading to high-performance solar cells. These results also demonstrate that an optimal water layer thickness significantly enhances the efficiency of Si solar cells without the need for complex design modifications [16,69,75] by reducing reflectance and improving light trapping. In addition, the consistent performance of the device across various light intensities highlights the reliability of the water immersion method for real-world applications.

2.4. Spectral optoelectronics and onsite power of immersed Si solar cells

In addition to the water layer thickness, the spectral characteristics of the Si PV device in air and water were investigated to clarify how water immersion affects the spectral performance of the device across different wavelengths. This analysis is crucial for understanding the broader implications of water immersion on the optoelectronic operation of Si solar cells, specifically for underwater photodetection and communication applications [76,77].

Pulsed light illumination at 50 Hz was applied to the Si solar cell in air and water, and J_{SC} profiles were recorded. Under UV light illumination (λ = 340 nm, 1.7 mW cm^{-2}), the J_{SC} value for the device increased from −0.339 in air to −0.423 mA cm^{-2} in water (Fig. 4a). However, under visible light illumination (λ = 530 nm, 6.8 mW cm^{-2}), the J_{SC} value of the device improved from −1.9 (in air) to −2.83 mA cm^{-2} (in water) as shown in Fig. 4b. Further, under IR illumination (λ = 850 nm), the immersed device showed improvements in its J_{SC} values from −12.11 (air) to −14.49 mA cm^{-2} (water) as shown in Fig. 4c.

The above results indicated that water immersion enhances photoresponse across all wavelengths relative to air operation. This improvement can be attributed to reduced Fresnel reflectance and light trapping provided by the water layer. Further, the photoresponse speed was consistent with that of water immersion. The rise and fall times of the photoresponse for the device were below 0.5 ms for all the UV, visible, and IR wavelengths in air and underwater (Fig. S3), confirming its underwater photoelectric applicability.

Incident-photon to current-conversion efficiency (IPCE) defines the quantum efficiency of a solar device as per the expression below.

$$IPCE(\lambda) = \frac{electrons\ cm^{-2}s}{photons\ cm^{-2}s} = \frac{J_{SC}(mA\ cm^{-2}) \times 1239.8\ (V\ nm)}{P_{hv}(mW\ cm^{-2}) \times \lambda(nm)} \quad (13)$$

where P_{hv} represents the intensity of light illumination.

Fig. 4d shows the relationship between IPCE, a critical metric that quantifies the efficiency of converting incident photons into electrical currents, and light wavelength for solar devices in air and water. From this figure, it is evident that water immersion significantly enhanced IPCE from 74 to 97.37 %, 72–96.7 %, and 80 to 96.07 for UV (340 nm), visible (530 nm), and IR (850 nm) wavelengths. The IPCE values estimated for illumination wavelengths 340, 365, 400, 430, 470, 530, 680, and 850 nm are summarized in Table S3.

The role of the water layer in driving more photons into the device was evident, resulting in a higher photocurrent owing to increased photon-to-carrier generation and collection. To provide clarification in this regard, we measured the reflectance profiles of the device in air and water using a diffused integrating sphere, as shown in Fig. 4e. The device was placed inside a quartz cuvette to obtain profiles. The results obtained revealed a decrease in reflectance, specifically in the UV and IR wavelength regions, suggesting that water plays a pivotal role by increasing the number of photons in the device.

Notably, we observed a decrease in IR wavelength reflectance below the Si bandgap, possibly owing to light absorption by the water layer, which prevented the induction of a thermal stimulus by the indirect bandgap structure. This phenomenon is further beneficial for PV operation as it lowered device temperature. The increased J_{SC} values and reduced surface reflection indicated that this improvement in the spectral IPCE across the UV–visible-IR wavelength range could be attributed to improved light absorption and charge carrier management resulting from water immersion.

The enhanced IPCE and reduced surface reflectance over a broad range of photon wavelengths suggested that water immersion helped drive more photons into the device. This minimized recombination losses via thermal regulation and improved IPCE performance, leading to an overall higher solar cell efficiency.

The onsite power characteristics of photovoltaic devices are particularly crucial for remote applications such as underwater power transmission. As water is transparent in the visible region, optical power transmission can be used to power underwater electronic and communication units. Fig. 4f summarizes the photovoltaic performance parameters, including V_{OC}, J_{SC}, FF, and PCE, for devices in air and water across different wavelengths (340, 365, 400, 430, 470, 530, 680, and 850 nm). These results are based on the J-V characteristics of the device in air and water at the optimal water layer thickness (Fig. S4 and Table S4) and indicated that water immersion consistently improved these performance parameters across the spectrum. The enhanced J_{SC} and V_{OC} values directly resulted from the improved light absorption and reduced recombination losses provided by the water layer. Additionally, the increased FF and PCE highlighted the effectiveness of water immersion in optimizing charge transport and minimizing losses within the device.

Taken together, water immersion significantly enhanced photoresponse and IPCE across different wavelengths, leading to improved J_{SC}, V_{OC}, FF, and PCE values. This improvement across the broadband spectrum highlights the reliability and potential of the water-immersion method for large-scale deployment. Additionally, these findings contribute to ongoing efforts to optimize PV technologies and pave the way for more efficient and reliable solar power generation.

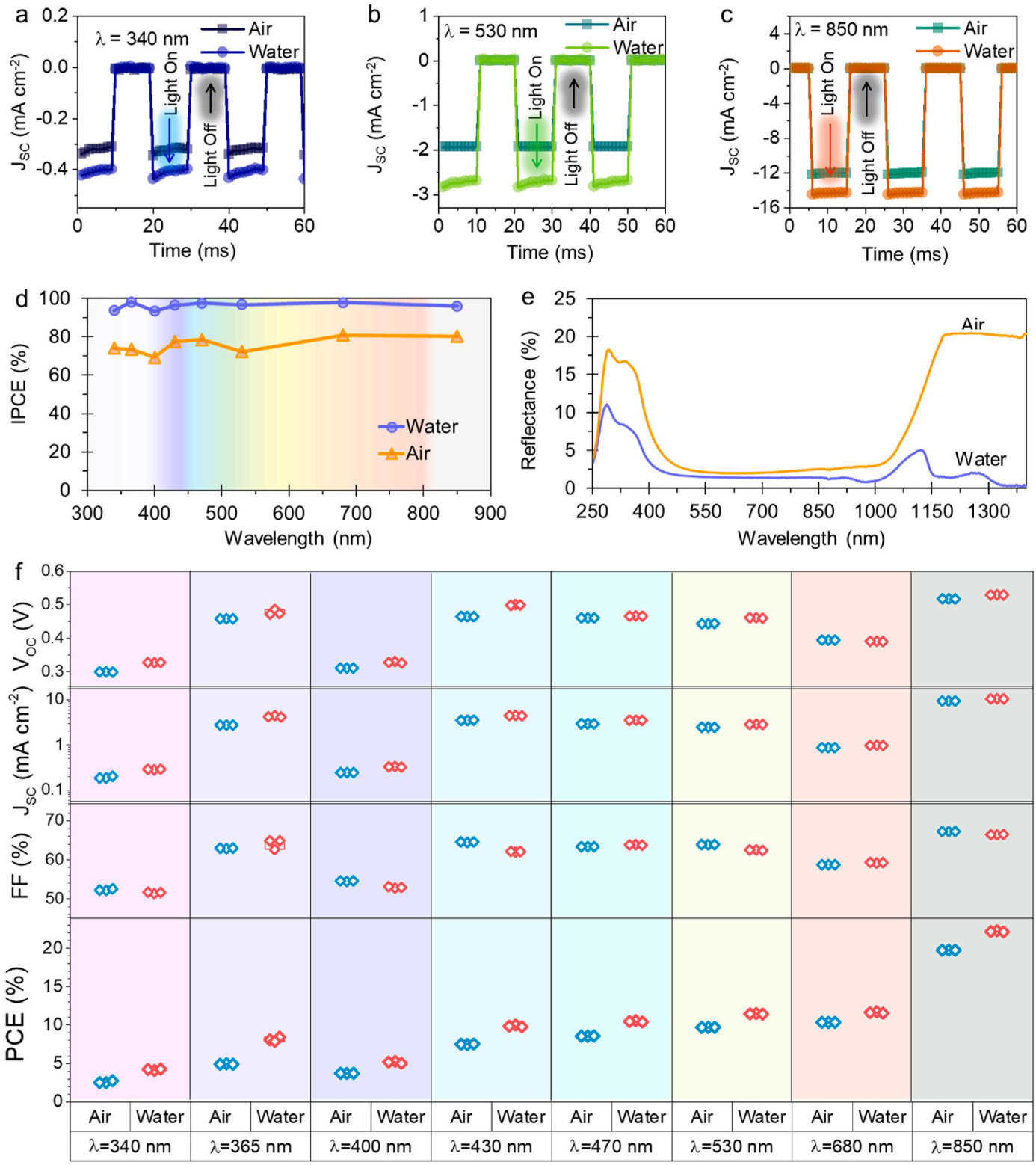

Fig. 4. Spectral characteristics of the Si PV cell in air and water. Photoresponses of the device in air and water with illumination wavelengths of (a) 340 nm for ultraviolet, (b) 530 nm for visible, and (c) 850 nm for infrared. (d) Variation of incident-photon to current-conversion efficiency (IPCE) with light wavelength for devices in air and water. (e) Reflectance spectra of the Si PV cell in air and water. (f) Summary of photovoltaic performance parameters of the Si device in air and water corresponding to the light illumination wavelength of 340, 365, 400, 430, 470, 530, 680, and 850 nm. These parameters were obtained from the current density-voltage (J–V) characteristics.

2.5. Thermal characteristics and steady power generation by the water-immersed device

Thermalization loss due to the photon energy being higher than the bandgap energy induces heating during prolonged operation of solar cells. According to the expression, $V_{OC} = \frac{kT}{q} ln\left(1 + \frac{J_{SC}}{J_0}\right)$, an increase in device temperature owing to thermalization heat results in a decrease in V_{OC}. This happens because of a significant increase in the dark saturation current in turn, degrades onsite power generation and conversion efficiency. Water emersion provides additional thermal radiation and

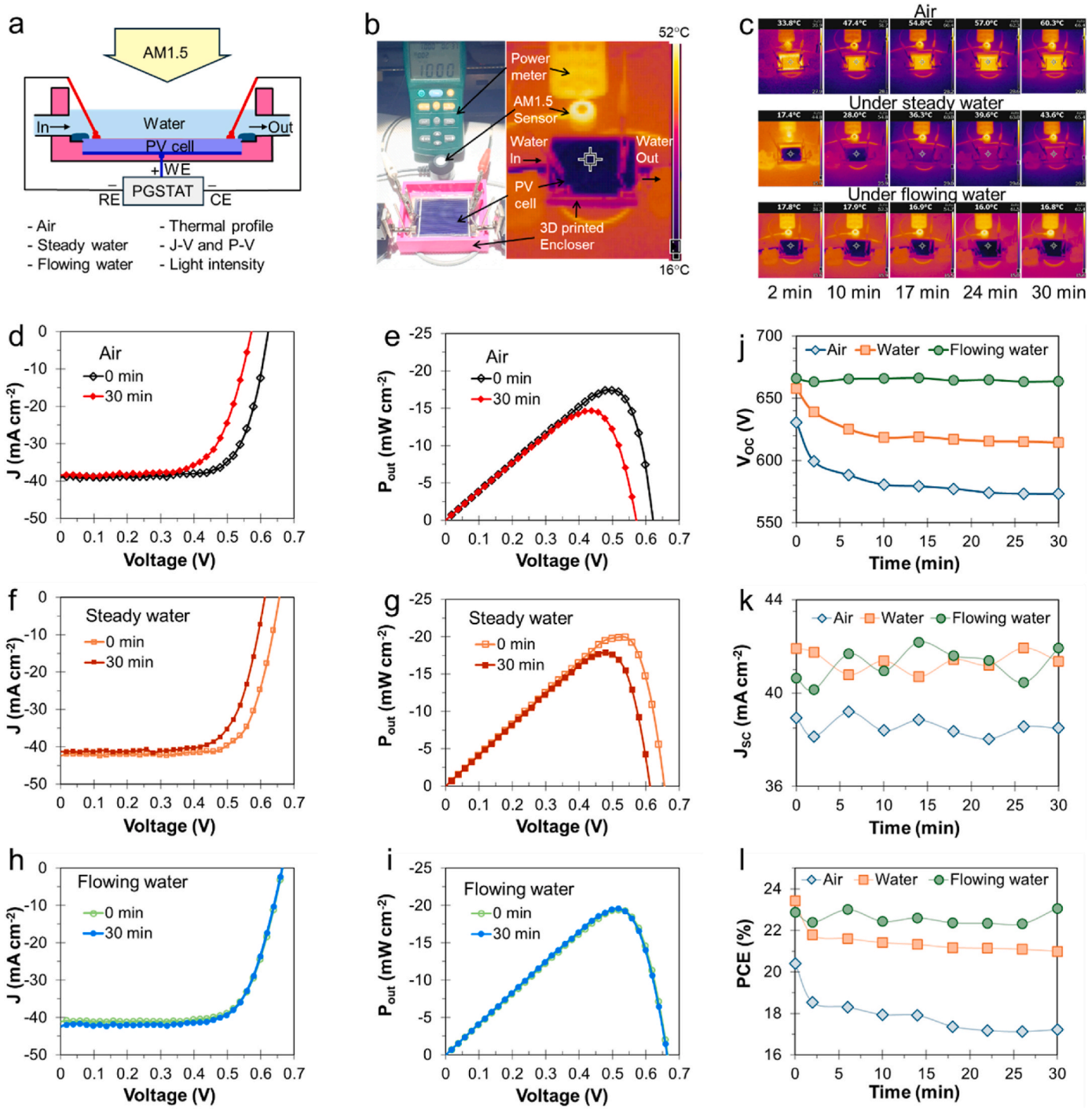

Fig. 5. Continued operation of solar cells under three conditions. (a) Schematic representation of the experimental design to investigate onsite power generation, thermal characteristics, and light intensity for solar cells in air and under steady and flowing water. (b) Original setup showing the Si solar cell in water under standard AM1.5 illumination with a solar power meter, photosensor, and 3D printed cell enclosure with water flowing and thermal profile of the setup with flowing water. (c) Thermal profiles showing temperature distribution of the device operating in air (top panel), steady water (middle panel), and flowing water (bottom panel) for 30 min with continuous AM1.5 illumination at 850 W m^{-2}. (d) Current density-voltage (J–V) characteristics and (e) power density-voltage (PV) characteristics of the device in air. (f) J-V and (g) P–V characteristics of the device in steady water. (h) J-V and (i) P–V characteristics of device in flowing water. Solar cell performance parameters as a function of operation time: (j) Open-circuit voltage (V_{OC}), (k) Short-circuit current density (J_{SC}), and (l) Power conversion efficiency (PCE).

dissipates heat while reducing Fresnel reflection. To further provide clarification in this regard, the thermal characteristics of the PV device in air and water were examined under continued operation under AM1.5G illumination.

Fig. 5a shows a schematic representation of the experimental setup used to study the thermal characteristics of the water-immersed solar cell. The setup included a 3D-printed underwater device enclosure, Si solar cell, solar power meter, and photosensor under standard light illumination. For qualitative assessment, onsite power generation was monitored via J-V and P–V characteristics synchronized with the light intensity and thermal profiles. The power generated by the device was measured in air, steady water, and flowing water.

Fig. 5b shows the original setup used to examine onsite power degradation and the thermal profile of the PV devices, depicting various components, including the flowing water profile. Further, Fig. 5c shows the time-elapsed thermal profiles of the setup. For device operation in air, we observed rapid heat gains, reaching 66.4 °C within 30 min of operation under continuous light illumination. In contrast, the thermal profiles of the device in steady water confirmed a lower solar cell temperature owing to the direct interface between the device and water. Heat transfer from the solar cells to water via thermal conduction increased the water temperature from 17 to 43.6 °C, potentially enabling water heating applications while lowering the solar cell temperature from 60.3 to 43.6 °C.

Interestingly, flowing water maintained a steady device temperature at approximately 17 °C, significantly lower than that observed in air and under the steady water scenario. This difference highlights the effective thermal management provided by the flowing water layer, functioning as a cooling medium and helping to dissipate heat more efficiently.

Sequential J-V characteristics were measured over a 30–min period to assess the effect of prolonged illumination on the PV characteristics of the device in air. Fig. 5d shows a significant degradation of the Voc value in air within 30 min of operation. Further, the P–V plot in Fig. 5e confirmed that the P_{max} decreased by 15.87 % (from 17.4 to 14.65 mW cm^{-2}) due to collective thermal degradation. The squareness of the J-V plots and the shift in the V_m value decreased over time, indicating a decrease in the FF value. The performance of the PV cell also decreased with time owing to thermalization-induced thermal stress.

In contrast, the device in steady water exhibited improved J_{SC} and V_{OC} values (Fig. 5f) as well as an increase in the P_{max} value to 19.92 mW cm^{-2} (Fig. 5g), with the temperature maintained below 44 °C. Thus, in steady water, the PV device only showed a 10 % decrease in power degradation within the 30-min operation period. This observation suggests better thermal management and reduces parasitic losses.

Moreover, the device under flowing water demonstrated excellent steady onsite power generation within the 30-min observation period, with J_{SC}, V_{OC}, and P_{max} values of 41.3 mA cm^{-2}, 665.5 mV, and 19.6 mW cm^{-2}, respectively (Fig. 5h and i). These results confirmed onsite power generation with less than 1 % variation under prolonged light illumination. Three consecutive cycles of prolonged light illumination also validated these results as shown in Fig. S5–S7, confirming stable onsite power delivery for 270 min, and these improvements could be directly attributed to the enhanced thermal management provided by the water layer, which helps maintain optimal thermal conditions and minimized parasitic losses caused by thermal degradation in the PV device.

Fig. 5j provides a summary of the V_{OC} of the device in air, steady water, and flowing water over time. The results showed that the V_{OC} of the device in air decreased rapidly from 630.3 to 580 mV within 10 min and thereafter, stabilized at 572.9 mV. In steady water, the V_{OC} increased to 657.8 mV and thereafter decreased slowly and stabilized at 614.3 mV. However, in flowing water, the V_{OC} was high and remained stable at 665.6 mV, owing to the excellent thermal control and improved diode properties provided by the following water at the water-Si device interface. This trend aligns with the improved thermal management and reduced recombination losses observed in the water-immersed devices. Fig. 5k provides a summary of the J_{SC} values of the device in air, steady water, and flowing water over time. From this figure, it is evident that steady and flowing water enhanced and stabilized J_{SC} values owing to improved optical losses. The FF of the device in air decreased from 70.7 % to 66.35 % (Fig. S8). However, under steady water and flowing water conditions, it remained stable in the range 70–72 %. Fig. 5l presents PCE as a function of operation time for the PV devices under the three test conditions. In air, PCE decreased significantly from 20.4 % to 17.21 % within 30 min of operation. In steady water, it was initially high PCE at 23.42 %, but decreased to 20.98 % with time. In flowing water, it remained stable at 22.87 %, demonstrating the effective management of thermal and optical losses through water immersion. The dark saturation current for a heavily n-doped junction is calculated according to the expression: $J_0 = qn_i^2\left(\frac{D_n}{L_n N_A}\right)$, where n_i, D_n, L_n, and N_A denote the intrinsic carrier concentration, electron diffusion coefficient, electron diffusion length, and acceptor carrier concentration, respectively, of the device [4]. Notably, J_0 is directly proportional to n_i^2, leading to a significant increase in temperature and a consequent decline in output power. The water-flow condition helped maintain the thermal state, providing an improved and stable power output probably owing to better thermal management, which stabilized V_{OC} (Eq. (8)) via more effective charge carrier management and a stable saturation current owing to the water layer.

The findings of this study emphasize the potential of water immersion in improving thermal management and enhancing the overall performance of Si solar cells. The results demonstrate that water immersion significantly reduces the operating temperature of the device, leading to more stable and higher J_{SC}, V_{OC}, and PCE values over prolonged operation. Therefore, water immersion presents as a simple and effective strategy for addressing thermal management challenges in PV technology. The stable performance of the water-immersed device across multiple conditions highlights the reliability and potential of water-immersion for large-scale deployment. These findings may contribute to ongoing efforts to optimize PV technologies and pave the way for more efficient and reliable solar power generation. Regarding concerns about water-induced degradation and the safety of electrical connections, we acknowledge that direct water contact necessitates an appropriate encapsulation strategy to protect the electrodes and ensure long-term durability. Furthermore, alternative water streams—including recycled water or even seawater—can be used, ensuring that the desired optical and thermal enhancements are achieved without exclusive reliance on clean water [47,67,78].

3. Conclusion

In this study, we investigated the effect of water immersion on the performance of Si PV cells. The results obtained indicated that a water layer, employed as an AR coating and thermal-treatment strategy, enhances the performance of commercial Si solar cells. Specifically, the water layer reduced Fresnel reflectance and improved light trapping, resulting in more efficient light absorption and an increase in the J_{SC} value of the device, hence a higher PCE. These improvements were also consistent across a broad spectrum of wavelengths and light intensities, as reflected by the enhanced photoresponses and IPCE of the water-immersed device. The optimal water layer thickness, 15 mm, further enhanced these benefits by minimizing optical loss and improving light management. Additionally, under standard AM1.5G illumination, the device showed a significant increase in PCE, highlighting the efficacy of the water immersion technique. Water immersion also provided effective thermal management, maintained lower operating temperatures, and reduced thermal stress, essential conditions for long-term stability and device performance. The stable J_{SC}, V_{OC}, and PCE values observed over prolonged operation demonstrated the potential of this method in enhancing the reliability of Si solar cells for continuous use. Under flowing water, the PCE of the device increased from 20.4 % to 22.8 % and provided stable on-site power generation with less than 1 %

variation over time.

These findings have important implications in the field of PVs, presenting water immersion as a simple, cost-effective, and scalable approach for improving the efficiency and reliability of Si solar cells. The consistent improvement in the key performance parameters across multiple devices suggested that the water immersion method is both reproducible and reliable, making it a promising candidate for large-scale deployment. These findings may also contribute to ongoing efforts to optimize PV technologies and promote the widespread adoption of renewable energy solutions. Future research should focus on further optimizing water immersion techniques, integration of encapsulation layer to protect against water degradation, possibility of using alternative water sources, modular design for outdoor conditions, and exploring its applicability to other photovoltaic technologies to drive more sustainable and energy-efficient innovations in the solar energy sector.

4. Materials and methods

4.1. Methods

Commercial 152 cm × 152 cm Si PV cells with polycrystalline p-Si and SiN_X AR coatings were used in this study. These devices have a p-n^+ junction with a certified PCE of 20 % under AM1.5G illumination at 300 K. Custom-sized devices (1.5 cm × 1.5 cm, 5.7 cm × 5.7 cm, and 4.4 cm × 6.5 cm) were fabricated using laser patterning (Cat-UV 5 W, Marcs, South Korea). The laser power, scan speed, and number of cycles were optimized for Si cell scribing to ensure electrical isolation and breakage-free cell cutting. For the underwater studies, tap water was applied to the front surface of the Si solar cells. Initially, the front and back contacts were isolated using Kapton tape to examine the diode properties of the device in air and water. Throughout this study, no modifications were made to the solar cells unless otherwise mentioned in the manuscript.

4.2. Water layer thickness and light intensity experiments

Water layer thickness experiments were performed using a home-built photoelectrochemical cell assembly composed of a Teflon material. The Si PV cell was assembled using an O-ring fixed to a stainless-steel back plate. The diameter of the O-ring, representing the working area, was 1 cm (0.785 cm^2) and the front contact constituted a gold-coated pogo pin immersed in water, while the back contact comprised a stainless-steel plate. The pogo-pin was aligned with a bus bar to ensure stability. Tap water was injected into the PV cell using a 5-ml syringe, with a cylindrical holder achieving predefined thicknesses of 1–29 mm. Further, the water layer thickness was varied successively to investigate its effect on the performance of the solar cell. For intensity studies, the optimal water thickness was applied and compared with the case without water.

For the electrical measurements, gold-coated tungsten pogo pins were connected to the reference and counter electrodes. The device was positioned under standard light illumination (AM1.5, McScience-K300, Korea), with the back electrode connected to the working and sensing electrodes. Fig. S9 shows the spectral characteristics of the AM1.5 light source. A PV power meter (McScience-K101, Korea) and a solar power meter with a data logger (TES-132 Solar Power Meter) were used to calibrate the solar simulator. The intensity of the light source was controlled by adjusting the lamp current from 10 to 50 A. Further, the light sensor was placed at the same height as the solar cell surface for accurate measurements, which were performed at room temperature (i.e., 300 K) and 50 % relative humidity.

To investigate the current density-voltage (J-V) and power density-voltage (P–V) characteristics of the solar cells, a potentiostat/galvanostat (PGStat, WonATech, ZIVE SP1) was used. PGStat was calibrated using standard LCR circuits before conducting the measurements. Linear sweep voltammetry was also performed within a voltage scan range of −0.2 to 0.7 V, at a scan speed of 0.2 V s^{-1}, at 20-mV intervals, with appropriate current compliance.

4.3. Spectral characteristics

The spectral characteristics of the Si PV cells in air and under the optimal water thickness were investigated using the aforementioned O-ring assembly. For the light source, light-emitting diodes emitting light at various wavelengths were integrated into a dual-adjustable power supply and function generator (Mightex WheeLEDTM, P/N: WLS-22-A). Light wavelengths of 340 nm (WLS-LED-0340-02), 365 nm (WLS-LED-0365-04), 400 nm (WLS-LED-0400-04), 410 nm (WLS-LED-0410-03), 460 nm (WLS-LED-0460-03), 520 nm (WLS-LED-0520-03), 625 nm (WLS-LED-0625-03), 730 nm (WLS-LED-0730-03), and 850 nm (WLS-LED-0850-03) were used. The light intensity of the visible wavelengths was calibrated using a standard Si photodiode, whereas the intensities at 340 and 365 nm were calibrated using a UV light meter (Lutron, UV-340A). The pulse illumination frequency was set to 50 Hz with the duty cycle at 50 %.

Chronoamperometry was employed to measure the transient current profiles of the devices under pulsed illumination at zero bias. The current range was custom-fitted according to the light intensity, and the sample period (1 ms) was set to burst mode. Fifty illumination pulses were recorded for the photoresponses and used to examine the incident photon-to-current conversion efficiency (IPCE) of the device in air and water.

To quantify the spectral PV performance of the solar cells, steady-state illumination at various wavelengths was employed and analysis was performed based on current density-voltage (J-V) and power density-voltage (P–V) characteristics. Three cycles were employed to verify the stable performance of the devices.

The reflectance spectra of the Si solar cells were determined using a UV–visible–NIR spectrophotometer (UV-2600; Shimadzu, Tokyo, Japan) equipped with a diffuse-reflectance integrating sphere. The device was immersed in tap water in a quartz cuvette, and the measurements were performed at 5-nm intervals. The reflectance baseline was established using a compressed $BaSO_4$ powder plate facing the incident light.

4.4. Investigation of the stable operation of solar cells

A time-elapsed underwater solar cell study was conducted to examine the operation of the PV device in air, steady water, and flowing water. The device (4.4 cm × 6.5 cm) was assembled into a 3D-printed enclosure with a water-flow arrangement. The back contact of the device comprised aluminum foil, while the front contact comprised a gold-coated pogo pin connected to the bus bar (at 5-cm spacings). The enclosure was designed using the Blender tool and printed using a 3D printer (Bambu Lab X1 Carbon Combo, Shenzhen, China). For the 3D printing, a PLA filament with a diameter of 1.75 mm was used, with the build plate temperature set at 100 °C and the tool head speed at 100 mm s^{-1}. Next, the Si solar cell was assembled using waterproof epoxy. The setup is as shown in Fig. 5b.

To observe the stability of the device, the solar simulator was pre-heated for 15 min and its performance was measured throughout the experiments. The temperature of the setup was measured in real time using a thermal imaging camera (Ti95 Thermal Imager, Fluke, Everett, WA, USA). For each run, a total exposure time of 30 min was considered to ensure reliable measurements. Three runs were performed to examine the solar cell performance parameters in air and under steady water and flowing water by recording J-V characteristic plots synchronized with a thermal camera and solar power meter at 2-min intervals.

CRediT authorship contribution statement

Malkeshkumar Patel: Writing – review & editing, Writing – original

draft, Validation, Resources, Methodology, Investigation, Formal analysis, Conceptualization. **Md Arifur Rahman Barno:** Visualization, Resources, Formal analysis. **Jessica Barichello:** Writing – review & editing, Validation, Resources, Investigation. **Sanh Vo Thi:** Visualization, Resources, Formal analysis. **Seunghee Cho:** Visualization, Formal analysis. **Fabio Matteocci:** Writing – review & editing, Validation, Supervision, Project administration. **Aldo Di Carlo:** Writing – review & editing, Validation, Supervision, Project administration, Funding acquisition. **Ching-Ping Wong:** Writing – review & editing, Supervision, Resources, Funding acquisition. **Joondong Kim:** Writing – review & editing, Validation, Supervision, Project administration, Conceptualization.

Declaration of competing interest

The authors declare that they have no known competing financial interests or personal relationships that could have appeared to influence the work reported in this paper.

Acknowledgments

The authors acknowledge the financial support of National Research Foundation of Korea (NRF) grant funded by the Korea government by the Ministry of Science and ICT (MSIT, RS-2024-0034883, NRF-2022R1I1A1A01054397) and Brain Pool Program (RS-2023-00283263).

Appendix B. Supplementary data

Supplementary data to this article can be found online at https://doi.org/10.1016/j.mtsust.2025.101158.

Data availability

Data will be made available on request.

References

[1] M.A. Green, S.P. Bremner, Energy conversion approaches and materials for high-efficiency photovoltaics, Nat. Mater. 16 (2017) 23–34, https://doi.org/10.1038/nmat4676.
[2] N.S. Lewis, Research opportunities to advance solar energy utilization, Science 351 (2016) aad1920, https://doi.org/10.1126/science.aad1920.
[3] P.K. Nayak, J. Bisquert, D. Cahen, Assessing possibilities and limits for solar cells, Adv. Mater. 23 (2011) 2870–2876, https://doi.org/10.1002/adma.201100877.
[4] A. McEvoy, T. Markvart, L. Castaner, Practical Handbook of Photovoltaics Fundamentals and Applications, second ed., Elsevier, 2012 https://doi.org/10.1016/C2011-0-05723-X.
[5] M.A. Green, E.D. Dunlop, M. Yoshita, N. Kopidakis, K. Bothe, G. Siefer, X. Hao, Solar cell efficiency tables (Version 63), Prog. Photovoltaics Res. Appl. 32 (2024) 3–13, https://doi.org/10.1002/pip.3750.
[6] Y. Li, X. Ru, M. Yang, Y. Zheng, S. Yin, C. Hong, F. Peng, M. Qu, C. Xue, J. Lu, L. Fang, C. Su, D. Chen, J. Xu, C. Yan, Z. Li, X. Xu, Z. Shao, Flexible silicon solar cells with high power-to-weight ratios, Nature 626 (2024) 105–110, https://doi.org/10.1038/s41586-023-06948-y.
[7] A. Polman, M. Knight, E.C. Garnett, B. Ehrler, W.C. Sinke, Photovoltaic materials: present efficiencies and future challenges, Science 352 (2016) aad4424, https://doi.org/10.1126/science.aad4424.
[8] S.Y. Khan, S. Rauf, S. Liu, W. Chen, Y. Shen, M. Kumar, Revolutionizing the solar photovoltaic efficiency: a comprehensive review on the cutting-edge thermal management methods for advanced and conventional solar photovoltaics, Energy Environ. Sci. (2025), https://doi.org/10.1039/d4ee03525a, 10.1039/d4ee03525a.
[9] T. Burger, C. Sempere, B. Roy-Layinde, A. Lenert, Present efficiencies and future opportunities in thermophotovoltaics, Joule 4 (2020) 1660–1680, https://doi.org/10.1016/j.joule.2020.06.021.
[10] M.A. Green, Crystalline and thin-film silicon solar cells: state of the art and future potential, Sol. Energy 74 (2003) 181–192, https://doi.org/10.1016/S0038-092X(03)00187-7.
[11] M.A. Green, How did solar cells get so cheap? Joule 3 (2019) 631–633, https://doi.org/10.1016/j.joule.2019.02.010.
[12] M.A. Green, Commercial progress and challenges for photovoltaics, Nat. Energy 1 (2016) 15015, https://doi.org/10.1038/nenergy.2015.15.
[13] J.A. Tsanakas, A. Heide, T. Radavičius, J. Denafas, E. Lemaire, K. Wang, J. Poortmans, E. Voroshazi, Towards a circular supply chain for PV modules: review of today's challenges in PV recycling, refurbishment and re-certification, Prog. Photovoltaics Res. Appl. 28 (2020) 454–464, https://doi.org/10.1002/pip.3193.
[14] A. Polman, H.A. Atwater, Photonic design principles for ultrahigh-efficiency photovoltaics, Nat. Mater. 11 (2012) 174–177, https://doi.org/10.1038/nmat3263.
[15] J.-H. Yun, E. Lee, H.-H. Park, D.-W. Kim, W.A. Anderson, J. Kim, N.M. Litchinitser, J. Zeng, J. Yi, M.M.D. Kumar, J. Sun, Incident light adjustable solar cell by periodic nanolens architecture, Sci. Rep. 4 (2015) 6879, https://doi.org/10.1038/srep06879.
[16] H.-S. Kim, D.B. Patel, H. Kim, M. Patel, K.R. Chauhan, W. Park, J. Kim, Electrical and optical properties of Si microwire solar cells, Sol. Energy Mater. Sol. Cells 164 (2017) 7–12, https://doi.org/10.1016/j.solmat.2017.01.046.
[17] H. Kim, J. Kim, E. Lee, D.W. Kim, J.H. Yun, J. Yi, Effect of the short collection length in silicon microscale wire solar cells, Appl. Phys. Lett. 102 (2013) 193904, https://doi.org/10.1063/1.4804581.
[18] W. Liu, Y. Liu, Z. Yang, C. Xu, X. Li, S. Huang, J. Shi, J. Du, A. Han, Y. Yang, G. Xu, J. Yu, J. Ling, J. Peng, L. Yu, B. Ding, Y. Gao, K. Jiang, Z. Li, Y. Yang, Z. Li, S. Lan, H. Fu, B. Fan, Y. Fu, W. He, F. Li, X. Song, Y. Zhou, Q. Shi, G. Wang, L. Guo, J. Kang, X. Yang, D. Li, Z. Wang, J. Li, S. Thoroddsen, R. Cai, F. Wei, G. Xing, Y. Xie, X. Liu, L. Zhang, F. Meng, Z. Di, Z. Liu, Flexible solar cells based on foldable silicon wafers with blunted edges, Nature 617 (2023) 717–723, https://doi.org/10.1038/s41586-023-05921-z.
[19] R. Saive, Light trapping in thin silicon solar cells: a review on fundamentals and technologies, Prog. Photovoltaics Res. Appl. 29 (2021) 1125–1137, https://doi.org/10.1002/pip.3440.
[20] E.C. Garnett, B. Ehrler, A. Polman, E. Alarcon-Llado, Photonics for photovoltaics: advances and opportunities, ACS Photonics 8 (2021) 61–70, https://doi.org/10.1021/acsphotonics.0c01045.
[21] O.E. Semonin, J.M. Luther, M.C. Beard, Quantum dots for next-generation photovoltaics, Mater. Today 15 (2012) 508–515, https://doi.org/10.1016/S1369-7021(12)70220-1.
[22] H.A. Atwater, A. Polman, Plasmonics for improved photovoltaic devices, Nat. Mater. 9 (2010) 205–213, https://doi.org/10.1038/nmat2629.
[23] J. Kim, M.D. Kumar, J.H. Yun, H.H. Park, E. Lee, D.W. Kim, H. Kim, M. Kim, J. Yi, H. Kim, C. Jeong, Transparent conductor-embedding nanolens for Si solar cells, Appl. Phys. Lett. 106 (2015) 151904, https://doi.org/10.1063/1.4918610.
[24] H.S. Kim, J.H. Yun, H.H. Park, M. David Kumar, J. Kim, Three-dimensional nanodome-printed transparent conductors for high-performing Si photodetectors, Mater. Lett. 148 (2015) 174–177, https://doi.org/10.1016/j.matlet.2015.02.090.
[25] Ruy S. Bonilla, B. Hoex, P. Hamer, P.R. Wilshaw, Dielectric surface passivation for silicon solar cells: a review, Phys. Status Solidi 214 (2017) 1700293, https://doi.org/10.1002/pssa.201700293.
[26] H. Savin, P. Repo, G. Von Gastrow, P. Ortega, E. Calle, M. Garín, R. Alcubilla, Black silicon solar cells with interdigitated back-contacts achieve 22.1% efficiency, Nat. Nanotechnol. 10 (2015) 624–628, https://doi.org/10.1038/nnano.2015.89.
[27] A. Shang, X. Zhai, C. Zhang, Y. Zhan, S. Wu, X. Li, Nanowire and nanohole silicon solar cells: a thorough optoelectronic evaluation, Prog. Photovoltaics Res. Appl. 23 (2015) 1734–1741, https://doi.org/10.1002/pip.2613.
[28] J. Oh, H.C. Yuan, H.M. Branz, An 18.2%-efficient black-silicon solar cell achieved through control of carrier recombination in nanostructures, Nat. Nanotechnol. 7 (2012) 743–748, https://doi.org/10.1038/nnano.2012.166.
[29] K.Q. Peng, X. Wang, L. Li, Y. Hu, S.T. Lee, Silicon nanowires for advanced energy conversion and storage, Nano Today 8 (2013) 75–97, https://doi.org/10.1016/j.nantod.2012.12.009.
[30] R. Verduci, V. Romano, G. Brunetti, N. Yaghoobi Nia, A. Di Carlo, G. D'Angelo, C. Ciminelli, Solar energy in space applications: review and technology perspectives, Adv. Energy Mater. 12 (2022) 2200125, https://doi.org/10.1002/aenm.202200125.
[31] L. Xu, E. Aydin, M. De Bastiani, M. Babics, J. Liu, R. Azmi, M. Alamer, M. F. Salvador, W. Liu, T. Allen, F. Xu, J. Kang, A. Subbiah, W. Yan, A.U. Rehman, L. Zhou, W. Raja, Q. Gan, Z. Liu, S. De Wolf, Parasitic heating of perovskite- and silicon-based photovoltaics, Adv. Energy Mater. 13 (2023) 2300013, https://doi.org/10.1002/aenm.202300013.
[32] L. Shen, Z. Li, T. Ma, Analysis of the power loss and quantification of the energy distribution in PV module, Appl. Energy 260 (2020) 114333, https://doi.org/10.1016/j.apenergy.2019.114333.
[33] S. Pescetelli, A. Agresti, G. Viskadouros, S. Razza, K. Rogdakis, I. Kalogerakis, E. Spiliarotis, E. Leonardi, P. Mariani, L. Sorbello, M. Pierro, C. Cornaro, S. Bellani, L. Najafi, B. Martín-García, A.E. Del Rio Castillo, R. Oropesa-Nuñez, M. Prato, S. Maranghi, M.L. Parisi, A. Sinicropi, R. Basosi, F. Bonaccorso, E. Kymakis, A. Di Carlo, Integration of two-dimensional materials-based perovskite solar panels into a stand-alone solar farm, Nat. Energy 7 (2022) 597–607, https://doi.org/10.1038/s41560-022-01035-4.
[34] E. Radziemska, The effect of temperature on the power drop in crystalline silicon solar cells, Renew. Energy 28 (2003) 1–12, https://doi.org/10.1016/S0960-1481(02)00015-0.
[35] E. Radziemska, Thermal performance of Si and GaAs based solar cells and modules: a review, Prog. Energy Combust. Sci. 29 (2003) 407–424, https://doi.org/10.1016/S0360-1285(03)00032-7.
[36] M.M. Rahman, M. Hasanuzzaman, N.A. Rahim, Effects of various parameters on PV-module power and efficiency, Energy Convers. Manag. 103 (2015) 348–358, https://doi.org/10.1016/j.enconman.2015.06.067.
[37] L. Xu, W. Liu, H. Liu, C. Ke, M. Wang, C. Zhang, E. Aydin, M. Al-Aswad, K. Kotsovos, I. Gereige, A. Al-Saggaf, A. Jamal, X. Yang, P. Wang, F. Laquai, T.

G. Allen, S. De Wolf, Heat generation and mitigation in silicon solar cells and modules, Joule 5 (2021) 631–645, https://doi.org/10.1016/j.joule.2021.01.012.
[38] M.A. Akrouch, K. Chahine, J. Faraj, F. Hachem, C. Castelain, M. Khaled, Advancements in cooling techniques for enhanced efficiency of solar photovoltaic panels: a detailed comprehensive review and innovative classification, Energy Built Environ 6 (2025) 248–276, https://doi.org/10.1016/j.enbenv.2023.11.002.
[39] H.G. Teo, P.S. Lee, M.N.A. Hawlader, An active cooling system for photovoltaic modules, Appl. Energy 90 (2012) 309–315, https://doi.org/10.1016/j.apenergy.2011.01.017.
[40] L. Chanphavong, V. Chanthaboune, S. Phommachanh, X. Vilaida, P. Bounyanite, Enhancement of performance and exergy analysis of a water-cooling solar photovoltaic panel, Total Environ. Res. Themes. 3–4 (2022) 100018, https://doi.org/10.1016/j.totert.2022.100018.
[41] K. Sukarno, A.S.A. Hamid, H. Razali, J. Dayou, Evaluation on cooling effect on solar PV power output using Laminar H2O surface method, Int. J. Renew. Energy Resour. 7 (2017) 1213–1218, https://doi.org/10.20508/ijrer.v7i3.5966.g7152.
[42] K. Mostakim, M.R. Akbar, M.A. Islam, M.K. Islam, Integrated photovoltaic-thermal system utilizing front surface water cooling technique: an experimental performance response, Heliyon 10 (2024) e25300, https://doi.org/10.1016/j.heliyon.2024.e25300.
[43] B. Du, E. Hu, M. Kolhe, Performance analysis of water cooled concentrated photovoltaic (CPV) system, Renew. Sustain. Energy Rev. 16 (2012) 6732–6736, https://doi.org/10.1016/j.rser.2012.09.007.
[44] Y. Wang, Z. Fang, L. Zhu, Q. Huang, Y. Zhang, Z. Zhang, The performance of silicon solar cells operated in liquids, Appl. Energy 86 (2009) 1037–1042, https://doi.org/10.1016/j.apenergy.2008.08.020.
[45] X. Han, Y. Wang, L. Zhu, The performance and long-term stability of silicon concentrator solar cells immersed in dielectric liquids, Energy Convers. Manag. 66 (2013) 189–198, https://doi.org/10.1016/j.enconman.2012.10.009.
[46] Y. Sun, Y. Wang, L. Zhu, B. Yin, H. Xiang, Q. Huang, Direct liquid-immersion cooling of concentrator silicon solar cells in a linear concentrating photovoltaic receiver, Energy 65 (2014) 264–271, https://doi.org/10.1016/j.energy.2013.11.063.
[47] A. Ghosh, A comprehensive review of water based PV: flotavoltaics, under water, offshore & canal top, Ocean Eng. 281 (2023) 115044, https://doi.org/10.1016/j.oceaneng.2023.115044.
[48] L. Zhu, R.F. Boehm, Y. Wang, C. Halford, Y. Sun, Water immersion cooling of PV cells in a high concentration system, Sol. Energy Mater. Sol. Cells 95 (2011) 538–545, https://doi.org/10.1016/j.solmat.2010.08.037.
[49] D. Vittorini, N. Castellucci, R. Cipollone, Heat recovery potential and electrical performances in-field investigation on a hybrid PVT module, Appl. Energy 205 (2017) 44–56, https://doi.org/10.1016/j.apenergy.2017.07.117.
[50] A. Ajitha, N.M. Kumar, X.X. Jiang, G.R. Reddy, A. Jayakumar, K. Praveen, T. Anil Kumar, Underwater performance of thin-film photovoltaic module immersed in shallow and deep waters along with possible applications, Results Phys. 15 (2019) 102768, https://doi.org/10.1016/j.rinp.2019.102768.
[51] X. Han, Y. Wang, L. Zhu, Electrical and thermal performance of silicon concentrator solar cells immersed in dielectric liquids, Appl. Energy 88 (2011) 4481–4489, https://doi.org/10.1016/j.apenergy.2011.05.037.
[52] N. Chander, Underwater performance evaluation of monocrystalline photovoltaic module in outdoor conditions and underwater spectral response study of c-Si solar cell, Silicon 15 (2023) 829–838, https://doi.org/10.1007/s12633-022-02063-1.
[53] S.K. Pathak, P.O. Sharma, V. Goel, S. Bhattacharyya, H.Ş. Aybar, J.P. Meyer, A detailed review on the performance of photovoltaic/thermal system using various cooling methods, Sustain. Energy Technol. Assessments 51 (2022) 101844, https://doi.org/10.1016/j.seta.2021.101844.
[54] R. Madurai Elavarasan, V. Mudgal, L. Selvamanohar, K. Wang, G. Huang, G. M. Shafiullah, C.N. Markides, K.S. Reddy, M. Nadarajah, Pathways toward high-efficiency solar photovoltaic thermal management for electrical, thermal and combined generation applications: a critical review, Energy Convers. Manag. 255 (2022) 115278, https://doi.org/10.1016/j.enconman.2022.115278.
[55] B. Sivakumar, S. Navakrishnan, M.R. Cibi, R. Senthil, Experimental study on the electrical performance of a solar photovoltaic panel by water immersion, Environ. Sci. Pollut. Res. 28 (2021) 42981–42989, https://doi.org/10.1007/s11356-021-15228-z.
[56] J. Walshe, P.M. Carron, S. McCormack, J. Doran, G. Amarandei, Organic luminescent down-shifting liquid beam splitters for hybrid photovoltaic-thermal (PVT) applications, Sol. Energy Mater. Sol. Cells 219 (2021) 110818, https://doi.org/10.1016/j.solmat.2020.110818.
[57] M. Chaplin, Water Absorption Spectrum (2013) 1–6. https://www.Chem.Uci.Edu/~unicorn/249/Handouts/Waterbands.Pdf. http://www.lsbu.ac.uk/water/vibrat.
[58] A. Shimkevich, Electrochemical view of the band gap of liquid water for any solution, World J. Condens. Matter Phys. 4 (2014) 243–249, https://doi.org/10.4236/wjcmp.2014.44027.
[59] A. Shimkevich, The hydrated-electron absorption spectrum in the view of the band theory of liquid water, J. Phys. Opt. Sci. 4 (2022) 1–5, https://doi.org/10.47363/JPSOS/2022(4)171.
[60] R. Paschotta, in: R.P. Photonics Encycl (Ed.), Fresnel Reflections - an Encyclopedia Article, RP Photonics AG, 2019, https://doi.org/10.61835/g7b.
[61] P.K. Enaganti, S. Nambi, H.K. Behera, P.K. Dwivedi, S. Kundu, M. Imamuddin, A. K. Srivastava, S. Goel, Performance analysis of submerged polycrystalline photovoltaic cell in varying water conditions, IEEE J. Photovoltaics 10 (2020) 531–538, https://doi.org/10.1109/JPHOTOV.2019.2958519.
[62] P.K. Enaganti, P.K. Dwivedi, R. Sudha, A.K. Srivastava, S. Goel, Underwater characterization and monitoring of amorphous and monocrystalline solar cells in diverse water settings, IEEE Sens. J. 20 (2020) 2730–2737, https://doi.org/10.1109/JSEN.2019.2952428.
[63] P.K. Enaganti, S. Goel, Investigation of silicon solar cells under submerged conditions with the influence of various parameters: a comparative study, Energy Technol. 9 (2021) 2100018, https://doi.org/10.1002/ente.202100018.
[64] K.K. Tse, T.T. Chow, Y. Su, Performance evaluation and economic analysis of a full scale water-based photovoltaic/thermal (PV/T) system in an office building, Energy Build. 122 (2016) 42–52, https://doi.org/10.1016/j.enbuild.2016.04.014.
[65] H.D. Fu, G. Pei, J. Ji, H. Long, T. Zhang, T.T. Chow, Experimental study of a photovoltaic solar-assisted heat-pump/heat-pipe system, Appl. Therm. Eng. 40 (2012) 343–350, https://doi.org/10.1016/j.applthermaleng.2012.02.036.
[66] Z.Z. Qiu, P. Li, T.T. Chow, Simulation of solar power system of building vertical photovoltaic glazing. Asia-Pacific Power Energy, Eng. Conf. APPEEC, 2009, pp. 1–4, https://doi.org/10.1109/APPEEC.2009.4918756.
[67] J.A. Röhr, B.E. Sartor, J. Lipton, A.D. Taylor, A dive into underwater solar cells, Nat. Photonics 17 (2023) 747–754, https://doi.org/10.1038/s41566-023-01276-z.
[68] O. Dupré, R. Vaillon, M.A. Green, Thermal behavior of photovoltaic devices: physics and engineering. https://doi.org/10.1007/978-3-319-49457-9, 2017.
[69] N. Kim, D. Choi, H. Kim, H. Um, K. Seo, Silicon microwire arrays with nanoscale spacing for radial junction c-Si solar cells with an efficiency of 20.5%, ACS Nano 15 (2021) 14756–14765, https://doi.org/10.1021/acsnano.1c04585.
[70] Q. Liang, X. Yan, Y. Gu, K. Zhang, M. Liang, S. Lu, X. Zheng, Y. Zhang, Highly transparent triboelectric nanogenerator for harvesting water-related energy reinforced by antireflection coating, Sci. Rep. 5 (2015) 9080, https://doi.org/10.1038/srep09080.
[71] Q.Z. Huang, J.F. Shi, L.L. Wang, Y.J. Li, L.W. Zhong, G. Xu, Study on sodium water glass-based anti-reflective film and its application in dye-sensitized solar cells, Thin Solid Films 610 (2016) 19–25, https://doi.org/10.1016/j.tsf.2016.05.010.
[72] M. Patel, S. Kim, J. Kim, Field-induced transparent electrode-integrated transparent solar cells and heater for active energy windows: broadband energy harvester, Adv. Sci. 10 (2023) 2303895, https://doi.org/10.1002/advs.202303895.
[73] S. Bowden, C. Honsberg, https://www.pveducation.org/pvcdrom/design-of-silicon-cells/light-trapping, https://www.Pveducation.Org/Pvcdrom/Welcome-to-Pvcdrom. (2016) 1–17. http://www.pveducation.org/pvcdrom/design/light-trapping.
[74] N Kumar, M Patel, TT Nguyen, S Kim, J Kim, Effect of TiO2 layer thickness of TiO2/NiO transparent photovoltaics, Progress in Photovoltaics: Research and Applications 29 (2021) 943–952.
[75] J. Kim, J.-H. Yun, H. Kim, Y. Cho, H.-H. Park, M.M.D. Kumar, J. Yi, W.A. Anderson, D.-W. Kim, Transparent conductor-embedding nanocones for selective emitters: optical and electrical improvements of Si solar cells, Sci. Rep. 5 (2015) 9256, https://doi.org/10.1038/srep09256.
[76] A. Ren, H. Wang, W. Zhang, J. Wu, Z. Wang, R.V. Penty, I.H. White, Emerging light-emitting diodes for next-generation data communications, Nat. Electron. 4 (2021) 559–572, https://doi.org/10.1038/s41928-021-00624-7.
[77] X. Gao, P. Liu, Q. Yin, H. Wang, J. Fu, F. Hu, Y. Jiang, H. Zhu, Y. Wang, Wireless light energy harvesting and communication in a waterproof GaN optoelectronic system, Commun. Eng. 1 (2022) 16, https://doi.org/10.1038/s44172-022-00016-5.
[78] C. Ma, Z. Liu, Water-surface photovoltaics: performance, utilization, and interactions with water eco-environment, Renew. Sustain. Energy Rev. 167 (2022) 112823, https://doi.org/10.1016/j.rser.2022.112823.